This paper can be found at https://link.springer.com/chapter/10.1007/978-3-030-76465-4_26

An analytical approach for pull-out behavior of TRM-strengthened rammed earth elements

Romanazzi A.[1], Oliveira D.V. [2] and Silva R.A.[3]

[1] ISISE & IB-S, University of Minho, Guimarães, Portugal, aromanazzi89@gmail.com
[2] ISISE & IB-S, University of Minho, Guimarães, Portugal, danvco@civil.uminho.pt
[3] ISISE & IB-S, University of Minho, Guimarães, Portugal, ruisilva@civil.uminho.pt

Abstract. Rammed earth constructions, beyond being largely spread in the built heritage, are known for their high seismic vulnerability, which results from high self-weight, lack of box behavior and low mechanical properties of the material. Hence, to mitigate this seismic vulnerability, a compatible textile reinforced mortar (TRM) is here proposed as a strengthening solution, because of its reduced mass and high ductility. The few research about the structural behavior of TRM-strengthened rammed earth elements addresses the global behavior, overlooking the local behavior of the system.
An analytical approach to infer the bond stress-slip relationship following the direct boundary problem is proposed. Based on a previous series of pull-out tests, an adhesion-friction constitutive law is portrayed considering also a damage model that considers the degradation of the reinforcing fibers due to friction.

Keywords: Rammed earth, textile reinforced mortar, bond, analytical approach

1 Introduction

Raw earth is one of the most ancient building materials and its related building techniques are spread worldwide, counting about 10% of the built UNESCO World Heritage and between 20% and 30% of the global population living in earthen dwellings [1][2]. Among the different building techniques based on the use of soil, rammed earth consists in compacting a mixture of moistened earth within a formwork, which is directly supported on the wall and moved horizontally once a block is completed [1]. This technique is used since ancient times to build both monuments [1][3] and affordable dwellings [4]. Nonetheless, rammed earth buildings are also well known for their high seismic vulnerability, which is due to low mechanical properties of the material, high self-weight and poor connection between structural elements. Thus, moderate to intense earthquakes are expected to produce in-plane cracking of the walls, formation of out-of-plane mechanisms and collapse of the roof and floors [5]. For this reason, textile reinforced mortar (TRM) has been proposed as a solution to mitigate

the high seismic vulnerability of rammed earth dwellings, due to its low self-weight, tensile strength and ductility, as demonstrated for masonry buildings [6]-[8].
Since the TRM is a composite system [6][9], understanding the mechanical response of the matrix-fiber interface is a key point to predict the overall performance of a strengthened structure. In this context, different test setups have been implemented to deduce the interaction between the two components [10]-[12]. Among these tests, the pull-out test is the most accepted, and consists in pulling out a single fiber or a mesh embedded in a specimen representing the matrix, while the corresponding load-displacement relationship *P(u)* is recorded. However, the *P(u)* curve is a response of a system with a specific geometry, not representing a material property of the tested composite. For obtaining material parameters to define the shear force transmission independently from the geometric properties, known as the bond stress-slip relationship (BSR), numerical or analytical models can be applied to the experimental *P(u)* curve [13][14]. In the case of cement-based matrix composites, an interface zone is assumed with properties different from the matrix and fiber [15]. As a consequence, if the stiffness of the interface is much smaller than that of the constituents, the deformation in this zone might be higher than that of the fiber u_f or matrix u_m. Therefore, the difference between the deformation of the components represents the interface deformation and it is defined as slip [$s=u_f-u_m$]. While, the bond stress-slip law is the transferred shear stress $\tau(s)$ as function of the slip (s) at the interface matrix-fiber at any coordinate of the fiber (x) [15]-[17][18].
In order to deduce the analytical law of the mortar-mesh interaction for imperfect interface models, two approaches have been implemented so far, namely a direct boundary problem (DBP) and an inverse boundary problem (IBP). In the case of the former approach, the load versus displacement relation *P(u)* of a pull-out test is calculated on the basis of an assumed constitutive law $\tau(s)$ [15][19]-[23]; therefore, its parameters must be supposed and the pull-out curve simulated to be compared with the experimental data. By means of fitting or an optimization process, the bond-slip law is verified once the best approximation is achieved.
The abovementioned approach is followed here to propose a method to infer a BSR of the experimental program conducted in Romanazzi *et al.* [24]. At first, the materials and the pull-out results of the experimental program are reported and discussed to hypothesize a BSR. Subsequently, the problem statement of the analytical model with the implementation of a novel damage model is derived.

2 Experimental program

The material properties and the results of a series of pull-out tests used to derive the BSR are reported in Romanazzi *et al.* [24]. The mechanical properties of the selected earth-based mortar were characterized according to EN 1015-11 [25]. The average flexural strength f_b is 0.5 MPa (CoV= 14%), while the compressive strength f_c is

1.2 MPa (CoV= 12%). The Young's modulus E_m was evaluated by means of axial compression tests on three cylindrical specimens of casted mortar with 90 mm of diameter and 175 mm high. The Young's modulus E_m was computed by linear fitting of the stress-strain curves in the range 0-30% of f_c, which provided an average value of about 4915 MPa (CoV= 20%). The tensile behaviour of the selected low-cost fiber glass mesh was evaluated according to the procedure prescribed in ASTM D6637 [26] and RILEM TC-250 CSM [27]. Five specimens were prepared with width of about 50 mm and with free length of 300 mm, considering the direction along which they show higher tensile capacity, as found in Oliveira *at al.* [28]. The resulting average maximum linear force $P_{w,p}$ is 18.4 kN/m (CoV 11%), while the average tensile strength f_t of a single yarn and the peak axial strain ε_{peak} are 626 MPa (CoV 11%) and 0.021 (CoV 10%), respectively. In addition, the average Young's modulus E_y is of about 32181 MPa (CoV 6%), as computed by linear fitting of the tensile stress-strain curve in the range 0-30% f_t. Table 1 summarizes the material properties.

Table 1. Properties of the selected glass fibre mesh and earth-based mortar.

Material	$P_{w,p}$ (kN/m)	ε_{peak} (-)	f_t (MPa)	E_y (MPa)	A_y (mm^2)	f_c (MPa)	f_b (MPa)	E_m (MPa)	A_m (mm^2)
Glass fiber mesh	18.4	0.021	626	32181	0.294	-	-	-	-
Earth mortar	-	-	-	-	-	1.2	0.50	4915	2.355

The pull-out specimens consisted of a glass fiber mesh band embedded in earth-based mortar cylinders with diameter of ±150 mm and height corresponding to the bonded length L_b. In the present study, only the specimens with bonded length 90 mm and 150 mm are considered. The specimens were casted ensuring the correct filling of the mold and perfect alignment of a single mesh band of 50 mm wide, while the unbonded part of the mesh was kept vertically to avoid any damage due to bending. The drying period of the specimens was of 28 days under constant hygrothermal conditions (T= 20±2 °C and RH= 60±5 %), after which they were subjected to displacement controlled pull-out tests. The displacements of the mesh were recorded by means of one LVDT set at the free end and two LVDTs set at the loaded end close to the mortar surface (see Figure 1). Further details are presented in Romanazzi *et al.* [24].

Figure 2a-d present the response curves in terms of force per width, displacement at the loaded end and displacement at the free end for the two different bonded lengths. Based on the literature [18][20][22][23][29][30], the experimental pull-out curves can be divided into two zones corresponding to different shear stress distributions along the interface. In particular, an initial linear response is observed, in which the load is

transmitted by adhesion. When the shear strength is achieved, micro-cracks are developed and the response becomes non-linear. In this stage, adhesion is still at the interface of the bonded fibers and friction between the two components is found in the detached part. As the shear strength is attained at the free end, friction becomes the only resistant mechanism.

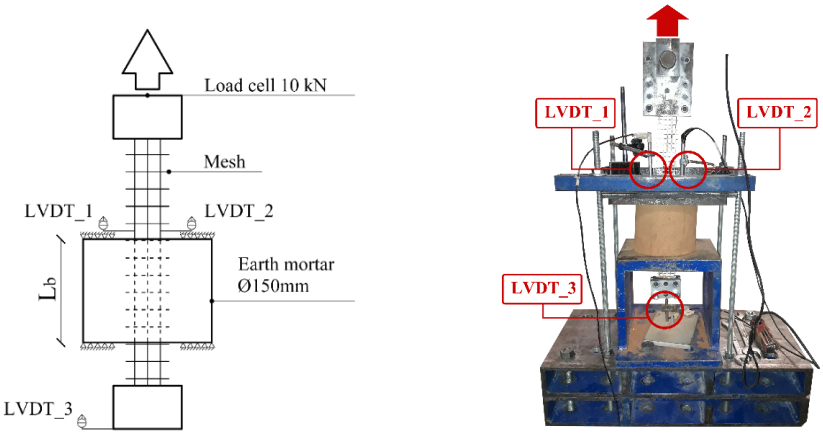

Figure 1. Setup of the pull-out tests.

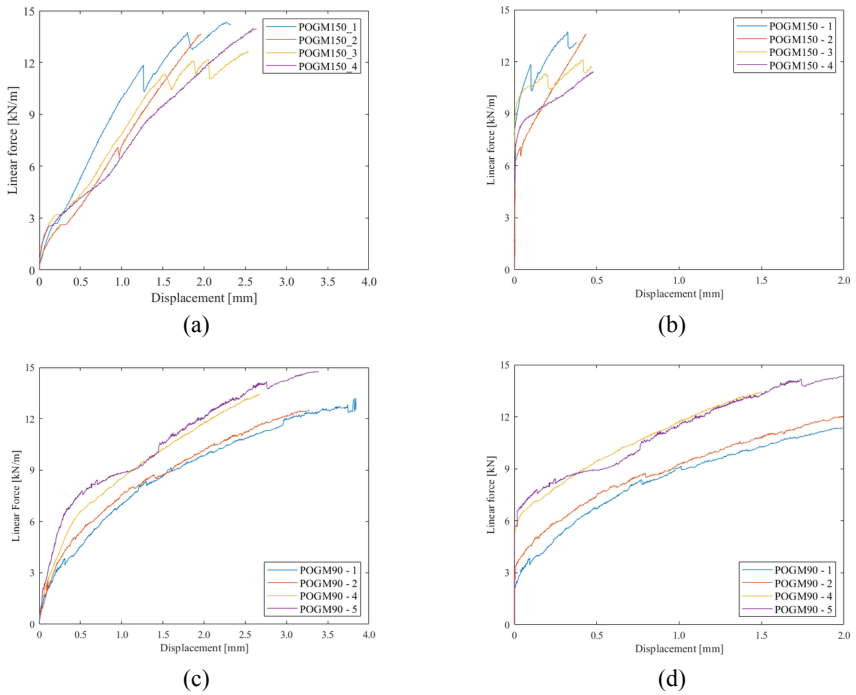

Figure 2. Pull-out experimental curves: (a) loaded end L_b 150 mm; (b) free end L_b 150 mm; (c) loaded end L_b 90 mm; (d) free end L_b 90 mm.

3 Analytical model

The direct approach was implemented for processing the experimental pull-out data and derive an analytical bond stress-slip law. Therefore, an adhesion-friction constitutive law was assumed with a linear response up to the maximum shear strength τ_{Max} and elastic slip s_{El}; subsequently, the strength drops to the shear friction resistance τ_{Fri} until failure (see Figure 3).

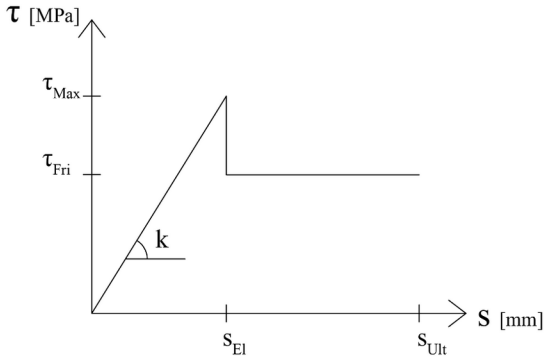

Figure 3. Assumed adhesion-friction bond stress-slip relationship.

Given the static equilibrium along the embedded length (Figure 4), the tensile force in the yarn F is transferred to the matrix M through the interface. Considering the infinitesimal interface dx, the equilibrium can be expressed as

$$\frac{dF}{dx} = -\frac{dM}{dx} = p\tau(x) \tag{1}$$

where p is the perimeter of the yarn and τ is the shear stress at the yarn-matrix interface.

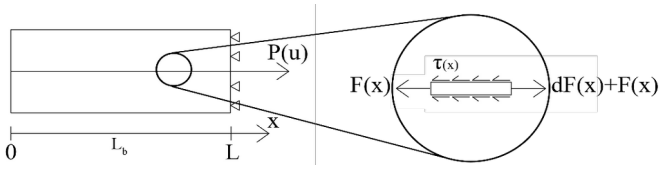

Figure 4. Static scheme of the interface during the pull-out test.

As the axial elongation in the fiber and in the matrix can be defined as $\varepsilon_{y=}\frac{F}{A_y E_y}$ and $\varepsilon_{m=}-\frac{F}{A_m E_m}$, the slip in the section x is the difference between the elongation of the components $s(x)=\frac{du}{dx}=\varepsilon_y-\varepsilon_m$, hence:

$$\frac{du}{dx}=\frac{F(x)}{A_y E_y}+\frac{F(x)}{A_m E_m} \tag{2}$$

where A_m, A_y, E_m and E_y are the cross section areas and Young's moduli of the matrix and fiber respectively. Substituting (2 into (1, one obtains:

$$\frac{dF}{dx}=\frac{d^2u}{dx^2}Q=p\tau \tag{3}$$

where $Q=\frac{1}{A_y E_y}+\frac{1}{A_m E_m}$ is the relative axial stiffness between the two components. (3 represents the analytical problem statement of the pull-out test to be solved according to the stage in which the section is, as described in the next section.

2.1. Linear stage

During the adhesion phase, the assumed interface stress-slip relationship is linear with $\tau=ku$ (Figure 3), which substituted in (3 leads to:

$$u''-\lambda^2 u=0 \tag{4}$$

with $\lambda=\sqrt{pkQ}$. The general solution of the second differential equation (4 is:

$$u(x)=C_1 e^{\lambda x}+C_2 e^{-\lambda x} \tag{5}$$

which substituted in (2 leads to:

$$F(x)=\frac{du}{dx}\frac{1}{Q}=\frac{1}{Q}\left(C_1\lambda e^{\lambda x}-C_2\lambda e^{-\lambda x}\right) \tag{6}$$

Considering as the boundary conditions the force in the fiber at the free-end, which is null $F(0)=0$, and the force in the fiber at the loaded-end, which is equal to the pull-out

force $F(L_b)=P$, the coefficients C_1 and C_2 result as $C_1 = C_2 = \frac{PQ}{\lambda(e^{\lambda L} - e^{-\lambda L})}$; which replaced in (6 gives the force distribution along the fiber $F(x)$ as:

$$F(x) = P\frac{(e^{\lambda x} - e^{-\lambda x})}{(e^{\lambda L_b} - e^{-\lambda L_b})} = P\frac{sinh(\lambda x)}{sinh(\lambda L_b)} \tag{7}$$

while the shear $\tau(x)$ and slip $s(x)$ distribution along the interface are respectively:

$$\tau(x) = \frac{dF}{dx}\frac{1}{p} = P\frac{\lambda}{p}\frac{cosh(\lambda x)}{sinh(\lambda L_b)} \tag{8}$$

and

$$u(x) = \int_0^x F(x)Qdx = PQ\frac{1}{sinh(\lambda L_b)}\int_0^x sinh(\lambda x)dx \tag{9}$$

For pull-out loads lower than the elastic limit load $F(L_b)=P<P_{El}$, the shear stress at the interface is less than the shear strength τ_{Max} and the yarn and the matrix are full bonded. Once the pull-out force achieves the elastic load $F(L_b)=P=P_{El}$, the shear strength τ_{Max} is attained at the loaded end $x=L_b$ and the debonding onsets. Hence, in such configuration the shear stress distribution is illustrated in Figure 5 and (8 becomes (10.

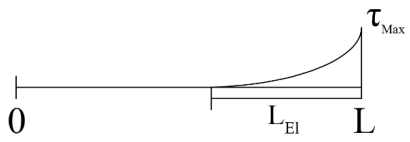

Figure 5. Shear stress distribution along the interface at elastic load.

$$\tau(L_b) = \tau_{max} = P_{El}\frac{\lambda}{p}\frac{cosh(\lambda L_b)}{sinh(\lambda L_b)} \tag{10}$$

While the slip at the loaded-end results:

$$s(L_b) = u_{El} = \int_0^{L_b} F(x)Qdx = P_{El}Q\frac{1}{sinh(\lambda L_b)}\frac{1}{\lambda}[\cosh(\lambda L_b) - 1] \tag{11}$$

Therefore, given the experimental elastic pull-out load and displacement (P_{El} and u_{El}), the shear strength [τ_{Max}] and the shear stiffness of the interface [k] are obtained by

solving the system of equations (10 and (11 at the coordinate of the loaded end ($x=L_b$).

2.2. Nonlinear stage

For loads beyond the elastic limit $F(L_b)=P>P_{El}$, the micro-cracks propagate along the interface toward the free-end. Consequently, the fiber and mortar are detached in the length L_d, while they are still bonded in the remaining length L_b-L_d. The resulted shear stress distribution is composed by constant frictional stress τ_{Fri} in the debonding length $L_d<x<L_b$ and adhesion $\tau=ku$ along the bonded length $0<x<L_b-L_d$, while the maximum shear strength τ_{Fri} is achieved at the coordinate $x=L_b-L_d$ (Figure 6).

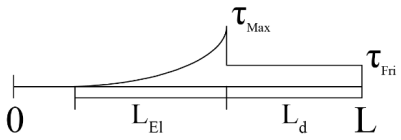

Figure 6. Shear stress distribution along the interface during nonlinear response.

Therefore, the pull-out force is the sum of the forces resulting from adhesion and friction as:

$$F(L_b) = P = F_{I_{max}} + F_{II} = \frac{\tau_{max}\, p}{\lambda} tanh[\lambda(L_b - L_d)] + \tau_{fri} p L_d \tag{12}$$

In this case, the boundary conditions are:

- $F(0)=0$
  $F(L_b - L_d) = \frac{\tau_{max}\, p}{\lambda} tanh\,[\lambda(L_b - L_d)]$
-
- $F(L_b)=P$

Which, placed in (3, lead to the force distribution $F(x)$ in the elastic length ($0<x<L_b-L_d$) as:

$$F_I(x) = \frac{\tau_{max}\, p}{\lambda} tanh[\lambda(L_b - L_d)] \frac{sinh(\lambda x)}{sinh[\lambda(L_b - L_d)]} \tag{13}$$

And in the debonded length ($L_b-L_d<x<L_b$):

$$F(x) = F_{I_{max}} + F_{II} = \frac{\tau_{max}\, p}{\lambda} tanh[\lambda(L_b - L_d)] + \tau_{fri} p(x - L_b + L_d) \tag{14}$$

The slip along the yarn *s(x)* can be evaluated as the sum of the slips according to the different stage in which the two parts of the yarns are. Therefore, the total slip at the loaded end results

$$s(L_b) = s_{El} + s_{Fri} = \\ = \frac{F_{l_{max}} \lambda Q}{sinh[\lambda(L_b - L_d)]}[cosh[\lambda(L_b - L_d)] - 1] + L_d Q\left(F_{l_{max}} + \frac{\tau_{fri} p L_d}{2}\right) \quad (15)$$

In this configuration, the debonded length L_d and the shear friction τ_{Fri} can be obtained by solving the system of equations (12 and (15, in which the inputs are the experimental pull-out force *P* and slip *u* in the nonlinear branch of the curve.

2.3. Damage model

Observing the experimental pull-out curve, a damage in the yarn due to the friction between mortar and fiber is deemed, as discussed in previous investigation [24]. In view of that, a damage model that considers the reduction of the cross-section of the yarn is introduced as function of the sliding. The damage is defined as $\xi(u) = \frac{A_y - A_{y_{Red}}}{A_y} x100$, where A_y and A_{yRed} represent the initial cross-section area (undamaged state) and the reduced cross section area of the yarn due to friction action, respectively. Considering the experimental ultimate load, the reduced section is evaluated as $A_{y_{Red}} = \frac{P_{Ult}}{n^\circ f_t}$, where f_t is the tensile strength of the dry mesh and *n* is the number of yarns. Afterwards, a correlation between the average value of damage and the bonded length (Figure 7a) and the sliding during the nonlinear stage (Figure 7b) was found and expressed in (16.

$$\xi = 2.3772 e^{1.0497(u_{Ult} - u_{El})} X \frac{1}{100} \quad (16)$$

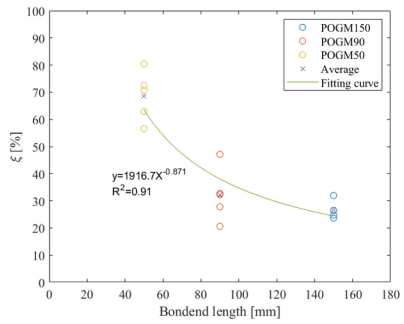

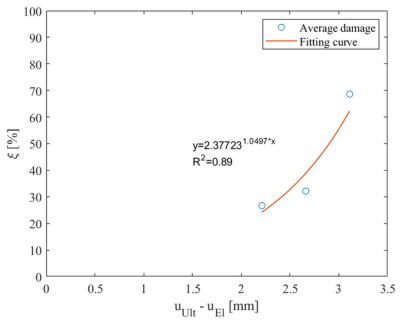

(a) (b)

Figure 7. Experimental correlations: (a) damage-bonded length; (b) damage-sliding in the non-linear stage.

Therefore, the value of $[1-\xi(u)]$, with $\xi(u) = 2.3772e^{1.0497(u-u_{El})}X\frac{1}{100}$, is introduced as factor to reduce the cross section of the yarn to evaluate the relative stiffness *Q(u)* in 17, which is then considered in the system of equations composed of (12 and (15 for the nonlinear stage.

$$Q(u) = \frac{1}{A_y(1-\xi(u))E_y} + \frac{1}{A_m E_m} \tag{17}$$

4 Conclusions

A method to infer a bond stress-slip relationship (BSR) of a TRM-based solution for strengthening rammed earth is here proposed following the direct boundary problem. At first, the properties of the materials used in the composite and the pull-out tests are presented. Based on the test evidences, an adhesion-friction BSR is hypothesized. Consequently, the equations to describe the stress transmission along the interface are inferred for the linear and non-linear stage. Therefore, the BSR parameters will be obtained considering the experimental results. Observing a correlation between the level of sliding and the loss of resistance with respect to the dry mesh, a novel damage model is assumed, which reduces the axial stiffness of the interface.

The proposed method is being implemented in an algorithm for simulating the pull-out test, in which a sensitivity analysis on the BSR parameters will be conducted. Though, the presented method is expected to be an approach for different combination of materials, rather than a thorough model for any composite with the use of earth-based matrixes.

Acknowledgment

This work was partly financed by FEDER funds through the Operational Programme Competitiveness Factors (COMPETE 2020) and by national funds through the Foundation for Science and Technology (FCT) within the scope of project SafEarth - PTDC/ECM-EST/2777/2014 (POCI-01-0145-FEDER-016737). The support from grant SFRH/BD/131006/2017 is also acknowledged.

References

[1] Houben H., Guillaud H. (2008) Earth construction: a comprehensive guide. London, Intermediate Technology Publication.

[2] Silva R.A., Oliveira D.V., Miranda T., Cristelo N., Escobar M.C., Soares E. (2013) Rammed earth construction with granitic residual soils: The case study of northern Portugal. Construction and Building Materials, 47, 181-191.

[3] Jaquin P.A., Augarde C.E., Gerrard C.M. (2008) A chronological description of the spatial development of rammed earth techniques. International Journal of Architectural Heritage, 2, 377-400.

[4] Silva R.A., Mendes N., Oliveira D.V., Romanazzi A., Domínguez-Martínez O., Miranda, T. (2018) Evaluating the seismic behaviour of rammed earth buildings from Portugal: from simple tools to advanced approaches. Engineering Structures, 157, 144-156.

[5] Costa A.A., Varum H., Rodrigues H., Vasconcelos G. (2015) Seismic behaviour analysis and retrofitting of a row building. In Correia M., Lourenço P.B., Varum H., Seismic Retrofitting: Learning from vernacular architecture. London, Taylor and Francis Group.

[6] De Felice G., De Santis S., Garmendia L., Ghiassi B., Larringa P., Lourenço P.B., Oliveira D.V., Paolacci F., Papanicolaou C.G. (2014) Mortar-based systems for externally bonded strengthening of masonry. Materials and Structures, 47, 2021-2037.

[7] Ghiassi B., Marcari G., Oliveira D.V., Lourenço P.B. (2012) Numerical analysis of bond behavior between masonry bricks and composite materials. Engineering Structures, 43, 210- 220.

[8] Valluzzi M.R., Modena C., De Felice G. (2014) Current practice and open issues in strengthening historical buildings with composites. Materials and Structures, 47, 1971-1985.

[9] Righetti L., Edmondson V., Corradi M., Borri A. (2016) Fiberglass grids as sustainable reinforcement of historic masonry. Materials, 9, 1-17.

[10] Dalalbashi A., Ghiassi B., Oliverira D.V. and Freitas A. (2018) Effect of test setup on the fiber-to-mortar pull-out response in TRM composites: experimental and analytical modeling. Composites: Part B, 143, 250-268.

[11] D'Ambrisi A., Feo L. and Focacci F. (2013) Experimental analysis on bond between PBO-FRCM strengthening materials and concrete. Composites: Part B, 44, 524-532.

[12] Donnini J., Lancioni G. and Corinaldesi V. (2018) Failure modes in FRCM systems with dry and pre-impregnated carbon yarns: experiments and modeling. Composites: Part B, 140, 57-67.

[13] Soranakom C. and Mobasher B. (2009) Geometrical and mechanical aspects of fabric bonding and pullout in cement composites. Materials and Structures, 42, 765-777.

[14] Li Y., Bielak J., Hegger J. and Chudoba R. (2018) An incremental inverse analysis procedure for identification of bond-slip laws in composites applied to textile reinforced concrete. Composites: Part B, 137, 111-122.

[15] Banholzer B., Brameshuber W. and Jung W. (2005) Analytical simulation of pull-out tests: the direct problem. Cement and concrete composites, 27, 93-101.

[16] Banholzer B., Brameshuber W. and Jung W. (2006) Analytical simulation of pull-out tests: the inverse problem. Cement e concrete composites, 28, 564-571.

[17] Banholzer B. (2006) Bond of a strand in a cementitious matrix. Materials and structures, 39, 1015-1028.

[18] Sueki S., Soranalom C., Mobasher B., Member ASCE and Peled A. (2007) Pullout-slip response of fabrics embedded in a cement paste matrix. Journal of materials in civil engineering, 19, 718-727.

[19] Naaman A.E., Member ASCE, Namur G.G., Alwan J.M. and Najm H.S. (1991) Fiber pullout and bond slip. I: analytical study. Journal of structural engineering, 117, 2769-2790.

[20] Carozzi F.G., Colombi P., Fava G. and Poggi C. (2016) A cohesive interface crack model for the matrix–textile debonding in FRCM composites. Composite structures, 143, 230-241.

[21] Ferreira S.R., Martinelli E., Pepe M., Silva F.D. and Filo R.D.T. (2016) Inverse identification of the bond behavior for jute fibers in cementitious matrix. Compistes: Part B, 95, 440-452.

[22] D'Antino T., Colombi P., Carloni C. and Sneed L.H. (2018) Estimation of a matrix-fiber interface cohesive material law in FRCM-concrete joints. Composite structures, 193, 103-112.

[23] Focacci F., D'Antino T., Carloni C., Sneed L.H. and Pellegrino C. (2017) An indirect method to calibrate the interfacial cohesive material law for FRCM-concrete joints. Materials and design, 128, 206-217.

[24] Romanazzi A., Oliveira D.V. and Silva R.A. (2019) Experimental investigation on the bond behavior of a compatible TRM-based solution for rammed earth heritage. International Journal of Architectural Heritage, DOI: 10.1080/15583058.2019.1619881.

[25] BS EN 1015 (1999) Methods of test for mortar for masonry. Part:11 determination of flexural and compressive strength of hardened mortar.

[26] ASTM D6637 (2015) Standard test method for determining tensile properties of geogrids by the single or multi-rib tensile method.

[27] De Felice G., Aiello M.A., Caggegi C., Ceroni F., De Santis S., Garbin E., Gattesco N., Hojdys L., Krajewski P., Kwiecień A., Leone M., Lignola G.P., Mazzotti C., Oliveira D., Papanicolaou C., Poggi C., Triantafillou T., Valluzzi M.R., Viskovic A. (2018) Recommendation of RILEM Technical Committee 250-CSM: Test method for Textile Reinforced Mortar to substrate bond characterization . Materials and Structures, 51, 95.

[28] Oliveira D.V., Silva R.A., Barroso C., Lourenço P.B. (2018) Characterization of a compatible low cost strengthening solution based on the TRM Technique for Rammed Earth. Key Engineering Materials, 747, 150-157.

[29] Zhang X.B., Aljewifi H. and Li J. (2013) Failure behaviour investigation of continuous yarn reinforced cementitious composites. Construction and building materials, 47, 456-464.

[30] D'Antino T., Carloni C., Sneed L.H. and Pellegrino C. (2014) Matrix-fiber bond behavior in PBO FRCM composites: a fracture mechanics approach. Engineering fracture mechanics, 117, 94-111.